JACS
JOURNAL OF THE AMERICAN CHEMICAL SOCIETY
Article
pubs.acs.org/JACS

Quantum Mechanical/Molecular Mechanical Calculated Reactivity Networks Reveal How Cytochrome P450cam and Its T252A Mutant Select Their Oxidation Pathways

Binju Wang,[†] Chunsen Li,[‡,§] Kshatresh Dutta Dubey,[†] and Sason Shaik*[,†]

[†]Institute of Chemistry and The Lise Meitner-Minerva Center for Computational Quantum Chemistry, The Hebrew University of Jerusalem, 91904 Jerusalem, Israel

[‡]State Key Laboratory of Structural Chemistry, Fujian Institute of Research on the Structure of Matter, Chinese Academy of Sciences, Fuzhou, Fujian 350002, China

[§]Fujian Provincial Key Laboratory of Theoretical and Computational Chemistry, Xiamen, Fujian 361005, China

Supporting Information

ABSTRACT: Quantum mechanical/molecular mechanical calculations address the longstanding-question of a "second oxidant" in P450 enzymes wherein the proton-shuttle, which leads to formation of the "primary-oxidant" Compound I (Cpd I), was severed by mutating the crucial residue (in P450cam: Threonine-252-to-Alanine, hence T252A). Investigating the oxidant candidates Cpd I, ferric hydroperoxide, and ferric hydrogen peroxide ($Fe^{III}(O_2H_2)$), and their reactions, generates reactivity networks which enable us to rule out a "second oxidant" and at the same time identify *an additional coupling pathway* that is responsible for the epoxidation of 5-methylenylcamphor by the T252A mutant. In this "second-coupling pathway", the reaction starts with the $Fe^{III}(O_2H_2)$ intermediate, which transforms to Cpd I via a O−O homolysis/H-abstraction mechanism. The persistence of $Fe^{III}(O_2H_2)$ and its oxidative reactivity are shown to be determined by interplay of substrate and protein. The substrate 5-methylenylcamphor prevents H_2O_2 release, while the protein controls the $Fe^{III}(O_2H_2)$ conversion to Cpd I by nailing—through hydrogen-bonding interactions—the conformation of the $HO^{\bullet}$ radical produced during O−O homolysis. *This conformation prevents $HO^{\bullet}$ attack on the porphyrin's meso position, as in heme oxygenase, and prefers H-abstraction from $Fe^{IV}OH$ thereby generating H_2O + Cpd I.* Cpd I then performs substrate oxidations. Camphor cannot prevent H_2O_2 release and hence the T252A mutant does not oxidize camphor. This "second pathway" transpires also during H_2O_2 shunting of the cycle of wild-type P450cam, where the additional hydrogen-bonding with Thr252 prevents H_2O_2 release, and contributes to a successful Cpd I formation. The present results lead to a revised catalytic cycle of Cytochrome P450cam.

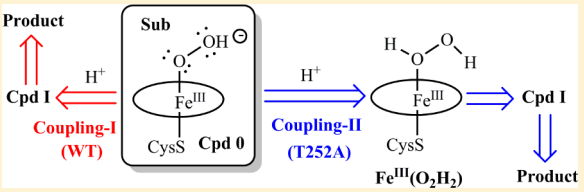

1. INTRODUCTION

Cytochromes P450 (CYPs) are versatile heme enzymes that catalyze a variety of oxygenations of organic substrates, such as hydroxylation, sulfoxidation and epoxidation reactions.[1−6] There is a consensus that the species responsible for these oxygenation reactions is the coupled high-valent iron(IV)−oxo porphyrin π-cation radicals species, the principal oxidant of the enzyme, so-called Compound I (Cpd I).[1−6] However, accumulating experimental results suggest[1,3a,7−16] the presence of a "second oxidant" in oxygenation reactions.

The issue of a second oxidant has known ups and downs.[3a,6−9] Nevertheless, the telltale experimental evidence for an additional oxidant species, besides Cpd I, has continued to linger. There are compelling results[8,9] which show that the substrate controls the outcome of the reactions in the T252A mutant of P450cam. Thus, in the presence of 5-methylenylcamphor (**S1**) the mutant enzyme leads to epoxidation of the C=C bond, whereas in the presence of the native substrate, camphor (**S2**) there is hardly any oxidation and the enzyme releases H_2O_2 ("uncoupling"). As such, our group, formerly an opponent of the idea,[5,17−20] had to face the accumulating critical evidence[7−13] for the presence of an additional oxidant species, and make an attempt to identify it.

In the present work we perform hybrid quantum mechanical/molecular mechanical (QM/MM) and molecular dynamics (MD) studies of CYP101, *so-called P450cam, and its T252A mutant*, wherein the proton-shuttle pathway for the conversion of Cpd 0 to Cpd I is severed. This mutant is likely to be the best candidate for finding such an additional oxidant, should such one exists. Using reaction-network schemes (e.g., Figure 4 later), which consider all the potential oxidants and pathways for epoxidation of **S1** in P450cam T252A, enables us to *identify the alternative coupling pathway in P450, in which the intermediacy of $Fe^{III}(O_2H_2)$ is indispensable.* The QM/MM-based reaction-networks show that the mutant enzymes do not involve a "second oxidant", but rather utilize a "second coupling pathway" that converts *$Fe^{III}(O_2H_2)$ to Cpd I in a manner that is both substrate and protein dependent.* It is shown that this new

Received: March 17, 2015
Published: May 26, 2015

DOI: 10.1021/jacs.5b02800
J. Am. Chem. Soc. 2015, 137, 7379−7390

picture is general and applicable also to the cases where the cycles of wild-type (WT) enzymes are shunted by peroxides.

2. BACKGROUND: THE CATALYTIC CYCLE OF P450

To provide an appropriate background, we show in Scheme 1 an abbreviated version of the consensus catalytic cycle by which

Scheme 1. Abbreviated Consensus Catalytic Cycle of P450

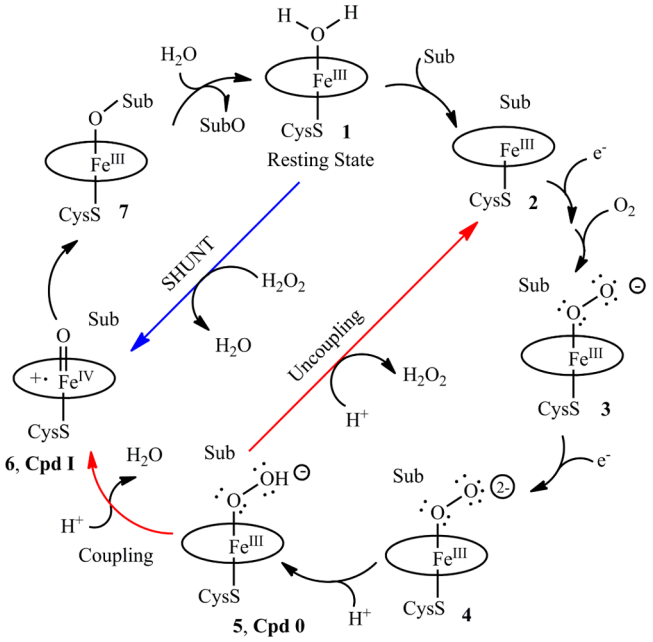

the P450cam and many other CYPs operate.[1−5] It starts with a resting state, which is generally the aqua-ferric complex **1**.

The cycle is gated by the entrance of the substrate (see Sub in **2** in Scheme 1), which expels the aqua ligand and other water molecules in the active site, and thereby elicits the reduction of **2** followed by O_2 uptake to generate the superoxide complex **3** (called also "oxyferrous") that undergoes a second reduction to form **4**. Being a very powerful base, **4** abstracts a proton and generates the ferric hydroperoxide species **5**, which is called also Compound 0 (Cpd 0).

As shown by the two red arrows in Scheme 1, Cpd 0 undergoes a second protonation. If this protonation occurs on the distal OH group, this will be attended by a liberation of a water molecule and formation of the species known as Cpd I.[4c] This species oxidizes the substrate and generates thereby the product complex Fe^{III}-OSub, **7**. Subsequently, the oxidized substrate is replaced by a water ligand to restore the resting state **1**. This is the major process in WT P450 enzymes.

If, however, the protonation of Cpd 0 occurs on the proximal oxygen, this leads to the formation of hydrogen peroxide that generally escapes the active site and thereby regenerates the ferriheme species, **2**. This process, in which substrate oxidation is aborted, is called also "uncoupling".[1−3,4a] The abortive H_2O_2 loss becomes dominant whenever the proton channel machinery, required for the O−O activation and formation of Cpd I, is disrupted. This disruption occurs by mutations of the acid/alcohol residues that shuttle protons through a water chain. In the case of P450cam, the crucial alcohol residue is Thr252. When this residue is replaced by Ala, this and analogous mutants still perform substrate oxygenation,[7−9] and in some cases even can lead to enhanced reactivity relative to the WT enzyme,[7] it is here where the second oxidant has been proposed, and as such, the T252A mutant is the focus of the present study.

The initial suggestions of the second oxidant focused on Cpd 0, however, this species was amply demonstrated to be unreactive, either in heme or in nonheme model systems.[17−23] Interestingly, nonheme Fe^{III}-OOH complexes bearing an *N*-methylated cyclam ligand, and possessing high spin-ground states, were found to lead to H-abstraction[24] and sulfoxidation[25] reactions. The other candidate of the "second oxidant" is the hydrogen peroxide complex, $Fe^{III}(O_2H_2)$ **8**. With rare exceptions,[16,26] **8** is not considered during normal catalysis, since hydrogen peroxide is a weakly bound ligand, and the formation of **8** should generally imply a loss of H_2O_2.[1−5,27]

However, there is crucial experimental evidence seemingly in favor of the presence of the ferric hydrogen peroxide complex **8** in the mutant enzyme. Thus, Dawson and Sligar[8] reported that the T252A mutant of P450cam had little if any activity in hydroxylation of camphor (**S2** in Scheme 2a), but it was still

Scheme 2. (a) Substrates S1 and S2, and (b) All Possible Transformation Pathways of Cpd 0/S1

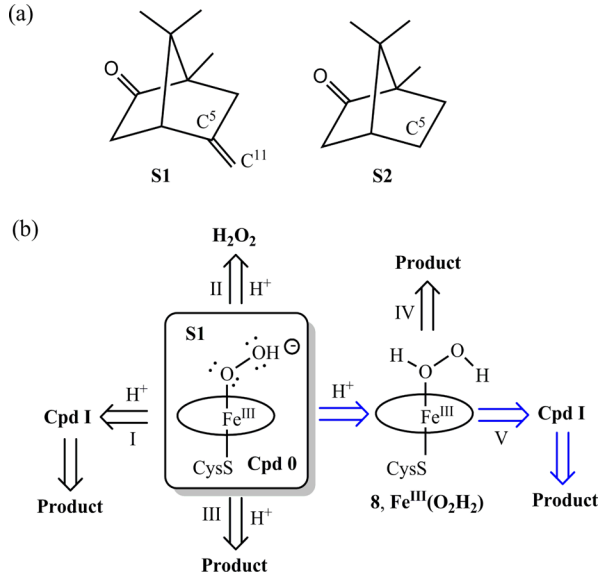

capable of epoxidizing 5-methylenylcamphor (**S1** in Scheme 2a). Subsequently, Davydov et al.[9] carried out cryogenic EPR/ENDOR investigation of the same mutant in the presence of a variety of substrates (including camphor, 5-methylenylcamphor, etc.). Davydov et al.[9] found that release of H_2O_2 was the major outcome (abortive uncoupling) in the T252A mutant of P450cam, when bound to **S2**. However, when the mutant enzyme was bound to **S1**, it caused primarily epoxidation of the substrate to the corresponding ethylene oxide.[9] As such, 5-methylenylcamphor (**S1**) may induce the formation of an intact $Fe^{III}(O_2H_2)$ **8** complex, which is potentially a strong oxidant that may lead to the epoxidation of the substrate via path IV in Scheme 2b. Alternatively, the lack of H_2O_2 liberation may arise from either, a hypothetical high reactivity of Cpd 0 in the presence of this substrate (path III) tacitly, or from the conversion of $Fe^{III}(O_2H_2)$ to Cpd I (path V), as is assumed to be happening during a typical shunt experiment[28−30] wherein H_2O_2 is used as a surrogate oxygen donor (see the blue arrow in Scheme 1).

DOI: 10.1021/jacs.5b02800
J. Am. Chem. Soc. 2015, 137, 7379−7390

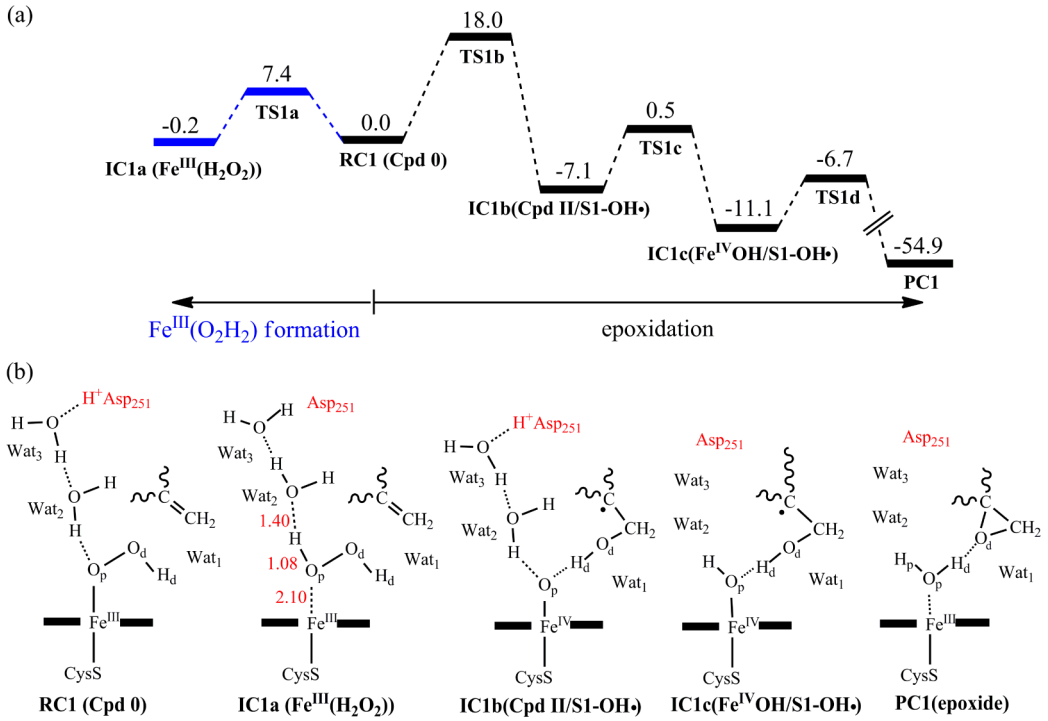

Figure 1. (a) QM/MM(UB3LYP/B2) relative energies (kcal/mol) for the competing reactions of Cpd 0 in the presence of **S1** (**RC1**). The blue energy profile to the left generates $Fe^{III}(O_2H_2)$. The black energy profile to the right describes the epoxidation of **S1** via the homolytic mechanism. (b) Schematic drawings of key intermediates along the reaction pathways. For **IC1a**, we show key bond distances (in Å).

As the above description shows, in answering the intriguing question, "which oxidant or pathway is really responsible for epoxidation of **S1** in the T252A mutant of P450cam", it is necessary to inspect all three candidates and their interconversion processes. This will be done here by usage of QM/MM calculations,[31,32] which lead to an atomistic description of structures and mechanism within the native environment of the protein,[33,34] and has been proven as a reliable method in numerous studies.[33−42]

Scheme 2 summarizes the targets of the QM/MM studies. Thus, we are going to consider all the possible candidates and pathways in the epoxidation of **S1**. By generating a full reactivity network of Cpd 0/**S1** as shown in Scheme 2b, our calculations can identify which oxidant or pathway is likely to be responsible for epoxidation of **S1** in T252A mutant of P450cam. Finally, we shall explore the substrate dependence,[8,9,43] namely why **S2** does not undergo much, if any, hydroxylation by the mutant, whereas **S1** undergoes substantial epoxidation? This result will be contrasted with the successful hydroxylation of **S2** by the WT enzyme using H_2O_2 shunt.[28]

As the following sections will show, considering the full reactivity networks of Cpd 0/**S1** in P450cam T252A will identify the exclusive pathway to epoxide product. In this pathway, our calculations show that the reaction proceeds via the $Fe^{III}(O_2H_2)$ intermediate, which then converts to Cpd I via the O−O homolysis/H-abstraction mechanism. It is Cpd I that is indeed responsible for the epoxidation of **S1** substrate. The difference between **S1** and **S2** in steering the reactivity of T252A will be discussed, and some generalizations will be made on the catalytic cycle of P450s.

3. COMPUTATIONAL METHODS AND DETAILS

3.1. Setup of the Cpd 0 and $Fe^{III}(O_2H_2)$ Systems and MD Runs. The initial structure of the enzyme−substrate complex was generated on the basis of the X-ray structure of camphor-containing P450cam (PDB code[44] 1dz9). Only chain A was kept while chain B was omitted. Thr252 was mutated into Ala252, while the axial H_2O ligand was converted into OOH group. Asp251 was protonated since it serves as the proton source in the subsequent transformations of Cpd 0, which has been well recognized by both experiment and theory.[1,3a,c,d,4a,5,44] Subsequently, following Altarsha et al.,[27] an extra water molecule (WatS) was added to connect the O_p of OOH group and the Asp251 residue, as shown in Figure 1b. The protonation states of titratable residues (His, Glu, Asp) were assigned on the basis of pK_a values based on PROPKA calculations[45] in combination with careful visual inspection of their local hydrogen bond networks. Solvation and protonation procedures followed the protocols in previous studies.[46] The resulting system had a net charge of 8$^-$, which was neutralized by protonating the titratable residues on the surface of the protein (the neutralization was shown to have little effect on the barrier of the rate-determining step, the O−O bond homolysis of $Fe^{III}(O_2H_2)$; see Figure S13). The generated neutral protein was solvated with a 16 Å layer of TIP3P water molecules (yielding a total of ca. 30 000 atoms). After these procedures, a productive MD run was performed for 20 ns for **S1** using the CHARMM22 force fields implemented in the CHARMM program.[47]

The $Fe^{III}(O_2H_2)$ system was set up based on the pre-built Cpd 0 model by changing the OOH moiety to HOOH. With $Fe^{III}(O_2H_2)$ inside the pocket, Asp251 is in its deprotonated state. Then, a productive MD run was performed for 20 ns for both **S1** and **S2** *by letting all the system fully relax*, and using published force field parameters for the Fe-O_2H_2 fragment.[48]

For the $Fe^{III}(O_2H_2)$ complex of the WT enzyme in the presence of **S2**, there was no need for an extra water molecule (WatS) to be added between H_2O_2 and Asp251.[27] All other features (except of course for the T252A mutation) were the same as in T252A mutant.

3.2. QM/MM Methodology. All QM/MM calculations were performed using ChemShell,[49] combining Turbomole[50] for the QM part and DL_POLY[51] for the MM part. The electronic embedding scheme[52] was used to account for the polarizing effect of the enzyme environment on the QM region. Hydrogen link atoms with the charge-shift model[49] were applied to treat the QM/MM boundary. In QM/

DOI: 10.1021/jacs.5b02800
J. Am. Chem. Soc. 2015, 137, 7379−7390

MM geometry optimizations, the QM region was treated by the hybrid UB3LYP[53] functional with two basis sets. A recent extensive benchmark study of H-abstraction by an iron-oxo species recommended the usage of UB3LYP as the best functional for such systems.[54]

For geometry optimization we used a basis set B1 consisting of 6-31G* for sulfur and LACVP for iron and 6-31G for other atoms. The energies were further corrected with the large all-electron basis-set def2-TZVP, labeled as B2. The CHARMM22 force field[55] was employed throughout this study for the MM region.

In general, we identify all the transition states (TSs) in two steps: first we trace the relaxed potential energy surface (PES) scans, which connect all the reactants, intermediates, and products rigorously. Then we take the saddle point structure to do full TS optimizations using the P-RFO optimizer implemented in the HDLC code.[56] In our past experience these two steps yield reasonably reliable TSs in QM/MM. For further checks, we carried out in the present work frequency calculations on the TSs of $Fe^{III}(O_2H_2)$ and Cpd I-mediated reactions (Figures S8−S10 and S16), and verified that all these TSs possess a single imaginary frequency.

We also tested the zero-point energy (ZPE) corrections for the $Fe^{III}(O_2H_2)$-mediated epoxidation reactions. As shown in Figure S11, the ZPE corrections systematically reduce the barrier by 0.8−1.6 kcal/mol. In the Cpd 0-mediated epoxidation reactions, the QM region (87 atoms) is significantly larger than $Fe^{III}(O_2H_2)$ systems (71 atoms), and the QM/MM frequency calculations are very time-consuming. Since the ZPE corrections for the $Fe^{III}(O_2H_2)$ reactions (Figure S11) do not affect any of the conclusions, these corrections are not expected to affect the analogous reactions of Cpd 0. As such, all the barriers in in the following sections are given without ZPE correction.

3.3. Choice of Spin States for the Reactions of Cpd I, Cpd 0, and $Fe^{III}(O_2H_2)$. As all the oxidants have a few closely lying spin states,[5] our first task was to determine the reactive-spin states. This is simple for Cpd 0 and Cpd I, which possess $S = {}^1/_2$ (doublet) ground states.[5] For Cpd 0, the $S = {}^3/_2$ (quartet) state lies significantly above $S = {}^1/_2$ and can be ignored for this study. For Cpd I, in most reactions, the $S = {}^3/_2$ and $S = {}^1/_2$ states exhibit rather similar barriers for bond activation reactions, such that no added information is provided by studying both states.[5] Furthermore, since Cpd I is generated from Cpd 0, it will anyway be formed in the $S = {}^1/_2$ state. As such, all the reactions of these two species were studied in the $S = {}^1/_2$ states.

$Fe^{III}(O_2H_2)$ is prepared in the cycle by protonation of Cpd 0 on the proximal O position of the OOH ligand (Scheme 2), and hence the ferric hydrogen peroxide complex will be generated in its $S = {}^1/_2$ state. $Fe^{III}(O_2H_2)$ has, however, three closely lying states, $S = {}^1/_2$ (doublet), $S = {}^3/_2$ (quartet) and $S = {}^5/_2$ (sextet), among which the doublet is the only reactive spin-state in oxidation processes.[20] This is verified here too by QM/MM calculations of the rate-determining step of $Fe^{III}(O_2H_2)$ reactions in the three different spin states (see Figure S12).

To explore the relative energies of the different spin states of $Fe^{III}(O_2H_2)$ in the P450cam protein environment, we computed all spin states using QM/MM with B2. The results are similar to the previous QM-only calculations,[20] namely, the ground state is $S = {}^5/_2$, which lies ca. 4.0 kcal/mol below the $S = {}^1/_2$ state (See Figure S21). The $S = {}^3/_2$ state lies in between. The Fe-Op bond lengths are 2.21, 2.79, and 2.80 Å for $S = {}^1/_2$, $S = {}^3/_2$ and $S = {}^5/_2$, respectively. As such, both $S = {}^3/_2$ and $S = {}^5/_2$ will preferentially liberate hydrogen peroxide, while $S = {}^1/_2$ will be the reactive state in substrate oxidation.

Nevertheless, since the spin-states dynamics may cause the generation of the higher spin states, this factor has at least to be considered. The crossing point between the $S = {}^1/_2$ and $S = {}^5/_2$ can be estimated[57] to lie ∼2 kcal/mol above the $S = {}^1/_2$ state. This is not much, but as $S = {}^1/_2$ and $S = {}^5/_2$ differ by two units of spin angular momentum, the direct spin−orbit coupling (SOC) is strictly zero,[58] and the two states can be coupled only indirectly through spin−orbit mixing with the $S = {}^3/_2$ state. One may therefore envision two potential scenarios: (i) if the spin inversion probability (SIP) is negligible, then the crossover will be slow, and the prepared $S = {}^1/_2$ of $Fe^{III}(O_2H_2)$ will perform primarily substrate oxidation, and (ii) if the SIP is efficient, then we might expect spin crossover from $S = {}^1/_2$ to $S = {}^3/_2$ and then to $S = {}^5/_2$. If the spin-crossover and H_2O_2 liberation are faster than the oxidation reaction of the $S = {}^1/_2$ state, then the reactive state will be depleted and the only outcome is H_2O_2 liberation. If, however, as in the case of **S1**,[9] the H_2O_2 liberation is not observed (since, as we show later, **S1** barricades H_2O_2,) there will then be pre-equilibrium between the spin states; as the Fe−O distance oscillates from long to short the $Fe^{III}(O_2H_2)$ complex will flip spin from $S = {}^5/_2$ to $S = {}^1/_2$ which will react further since it has the lowest barriers in its follow-up reactions (e.g., Figure S12). Thus, even if $Fe^{III}(O_2H_2)$ $S = {}^1/_2$ has only a minor population in the pre-equilibrium,[48] still the complex may participate in a follow-up reaction, especially when the latter is a thermodynamically favorable and hence an irreversible process. As shown later, $Fe^{III}(O_2H_2)$ $S = {}^1/_2$ is preferentially converted to Cpd I with the lowest barrier and in an exothermic reaction (−21.4 kcal/mol), such that the reaction is both kinetically and thermodynamically driven. We therefore proceed with the $S = {}^1/_2$ state of $Fe^{III}(O_2H_2)$.

Thus, based on the above discussion, the reactivities of Cpd 0, Cpd I, and $Fe^{III}(O_2H_2)$, were restricted to the respective $S = {}^1/_2$ states.

4. RESULTS AND DISCUSSION

4.1. Reactivity of Cpd 0 with S1. To study the reactivity of Cpd 0, Asp251 should be protonated since it has to serve as proton donor in the proton-shuttle reactions. [Note that Asp251 has access to the bulk water, and it can control the proton shuttle through a "carboxylate switch". As suggested long ago based on experimental considerations,[3c,d] the deprotonated Asp251 blocks the water entry, since it is engaged in salt bridges with Arg186, but upon protonation, Asp251 will flip to the inside of the active site and open the channel to water molecules. As shown before,[5] the protonation is quite facile, since Asp251 can rotate off the salt bridge by 40° at a small energy expense.] In accordance with the study of Altarsha et al.,[27] the protonated Asp251 forms a stable proton channel with the proximal oxygen O_p of Fe^{III}−OOH (Figure S1) throughout the MD simulation. Thus, in order to treat the system in an unbiased manner, all the surrounding water molecules as well as the protonated Asp251 were incorporated in the QM region as schematically shown in Figure 1.

Starting from the Cpd 0/substrate complex (**RC1**) species, there are generally three competing pathways. The first one is the Cpd I formation, which requires an initial H-bond shift from O_p to O_d followed by O−O cleavage of Cpd 0 to form Cpd I (Figure S2). In agreement with ref 27., the calculated barrier for Cpd I formation from Cpd 0 is high, 20.6 kcal/mol (Figure S2), and noncompetitive with formation of $Fe^{III}(O_2H_2)$. Figure 1a shows the other two competing pathways: one to the left in blue is the formation of the $Fe^{III}(O_2H_2)$ complex, the other to the right in black is the Cpd 0-mediated epoxidation. In the Cpd 0-mediated epoxidation, we present the homolytic cleavage pathway; the alternative concerted nucleophilic attack pathway exhibits a prohibitively high barrier (Figure S3), in consistency with previous QM-only model calculations.[20,22]

Consider first the blue energy profile for $Fe^{III}(O_2H_2)$ formation by proton transfer from Asp251 via the water chain (Wat 2, Wat 3) to the O_p site of Cpd 0 (Figure 1a). As was found before by Altarsha et al.[27] and here too, the so formed **IC1a** complex maintains a very strong hydrogen-bond (H-bond) with the chain of the two waters and the Asp251 anion, such that the O_p-H bond of H_2O_2 is elongated to 1.08 Å (also see in Figures S4), as if forming an intermediate state in between $Fe^{III}(O_2H_2)$ and Cpd 0. As shown by our MD simulations (Figure S7) of $Fe^{III}(O_2H_2)$, the negatively charged

DOI: 10.1021/jacs.5b02800
J. Am. Chem. Soc. 2015, 137, 7379−7390

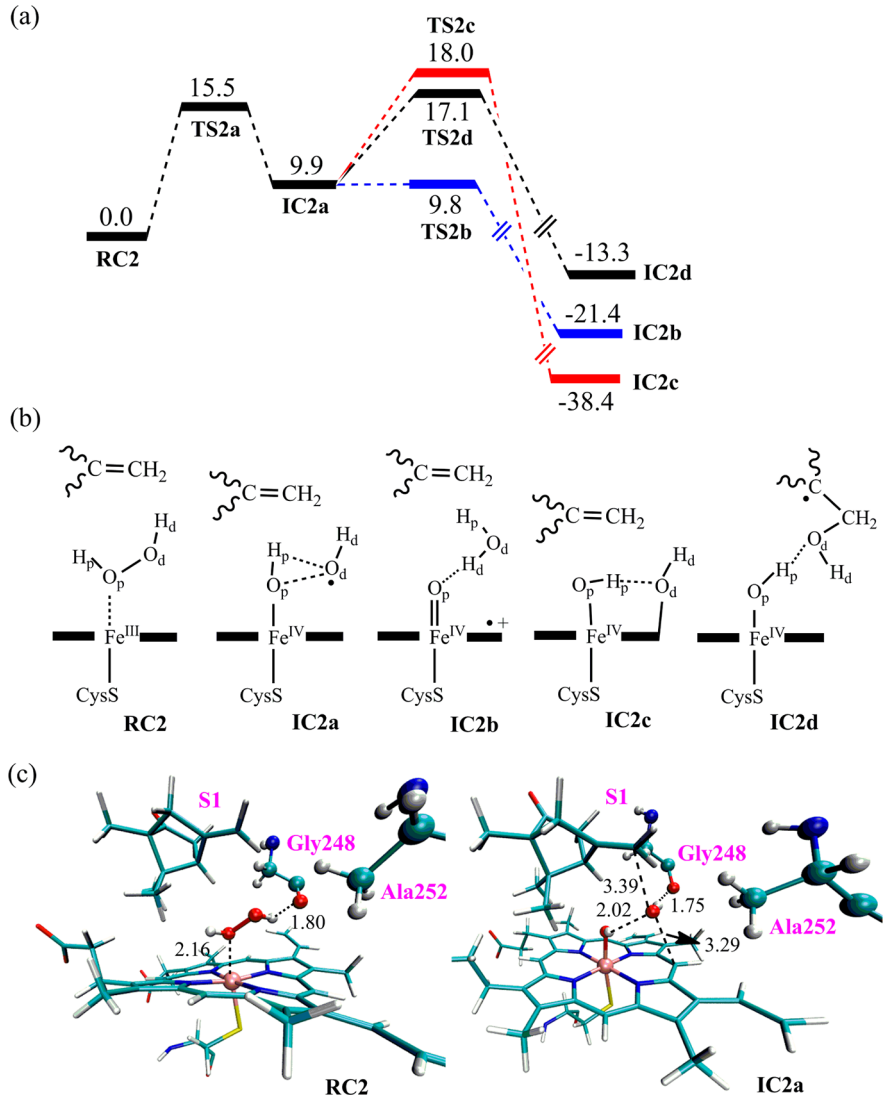

Figure 2. (a) UB3LYP/B2 relative QM/MM energies (kcal/mol) for the reactions of the $Fe^{III}(O_2H_2)$/**S1**. Starting from the protonated Cpd II/HO$^{\bullet}$ radical complex, **IC2a**, we show three competing follow-up pathways: the $^{\bullet}$OH radical abstracts an H atom from the iron hydroxo complex and leads to Cpd I (blue curve), or attacks the *meso*-position of the porphyrin (red curve), or adds to the double bond in **S1** (black curve). (b) Schematic drawings of key intermediates along the reaction pathways. (c) QM/MM optimized structures for the reactant complexes of $Fe^{III}(O_2H_2)$, **RC2**, and the respective intermediate complexes $Fe^{IV}OH$---$^{\bullet}$OH formed by O−O bond homolysis, **IC2a**. Key bond lengths are given in angstroms.

carboxylate of Asp251 will rotate quickly upward to make salt bridges with Arg186.[3c,d,5] This in turn leads to the breakage of the water chain (Wat2, Wat3) that connects to H_2O_2 by H-bonding, thus generating a fully formed $Fe^{III}(O_2H_2)$ complex with a normal O_p−H bond.

The black energy profile in Figure 1a depicts the mechanism for the epoxidation of **S1** via initial O−O bond homolysis of Cpd 0. Interestingly, the homolytic cleavage of the O−O bond occurs in concert with $^{\bullet}$OH radical attack on the double bond, leading to the radical intermediate (**IC1b**) that involves the hydroxylated radical, **S1**−OH$^{\bullet}$, and the Fe^{IV}=O^{-} species, so-called Compound II (Cpd II). This radical complex, Cpd II/**S1**−OH$^{\bullet}$, undergoes epoxide formation in two steps. Initially the O_p moiety of Cpd II abstracts a proton from Asp251 via the water chain, thus generating the complex PorFe^{IV}OH/**S1**−OH$^{\bullet}$, **IC1c**. Subsequently, C−O_d formation coupled with H_d shift to O_p leads to ring closure and epoxide product (**PC1**) formation.

Comparison of two pathways in Figure 1a shows that the $Fe^{III}(O_2H_2)$ formation is hugely favorable over the epoxidation pathway. Using two other snapshots (Figure S5 and S6), led to the same conclusion. *Thus, in the presence of the olefin substrate* ***S1****, the mutant's Cpd 0 will exclusively generate* $Fe^{III}(O_2H_2)$. Therefore, in accord with former QM results,[17−22] this computational evidence leads to the conclusion that Cpd 0 can be excluded as a potential oxidant in the T252A mutant of P450cam.

4.2. Reactivity of $Fe^{III}(O_2H_2)$ with S1. We considered the reactivity of the $Fe^{III}(O_2H_2)$ species, which is exclusively formed from the reaction of Cpd 0/**S1**. MD simulations showed the initial water chain between O_p of $Fe^{III}(O_2H_2)$ and the Asp251 anion is quite unstable. This water chain broke down quickly during the MD simulation even with gentle heating (Figure S7), and in the equilibrated structure Asp251 flipped far away and underwent strong H-bonding to Arg186, Thr185, and the nearby water molecules. Therefore, Asp251 is

DOI: 10.1021/jacs.5b02800
J. Am. Chem. Soc. 2015, 137, 7379−7390

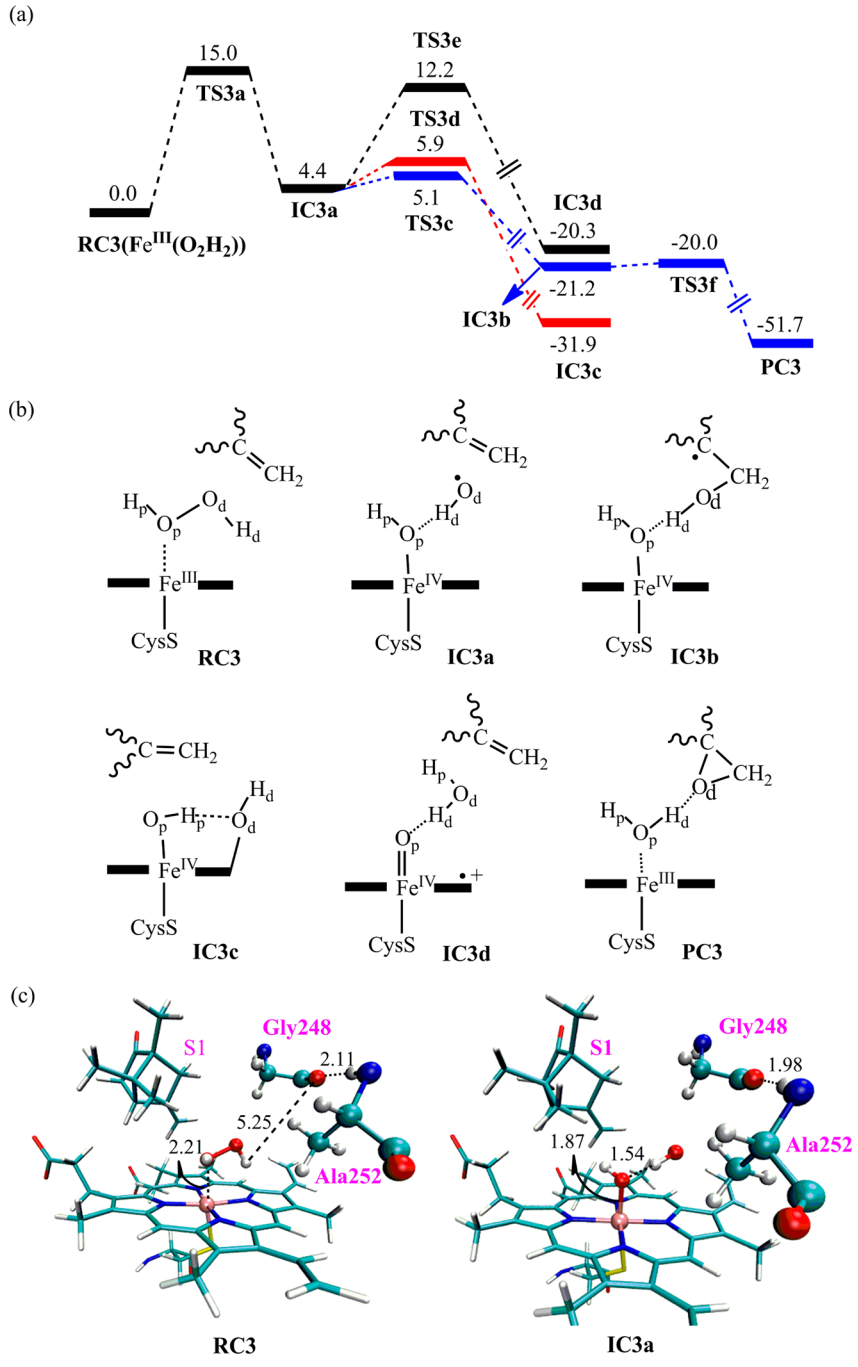

Figure 3. Importance of the conformation of the •OH Radical: (a) UB3LYP/B2 relative QM/MM energies (kcal/mol) for the reactions *of the constrained-Fe^{III}(O_2H_2) complex* in the presence of **S1**. Starting from the reactant complex, **RC3**, the homolysis of the O−O bond (black curve) yields the protonated Cpd II/HO• radical complex, **IC3a**. Starting from **IC3a**, the •OH radical abstracts an H atom from the iron hydroxo complex and leads to Cpd I (black curve), or attacks either the *meso*-position of the porphyrin (red curve), or the double bond in **S1** leading subsequently to the epoxide product (blue curve). (b) Schematic drawings of key intermediates along the reaction pathways. (c) QM/MM optimized structures for the reactant complexes of **RC3** and the intermediate complexes of **IC3a**. Key bond lengths are given in angstroms.

not expected to act as base catalyst in the following reactions of Fe^{III}(O_2H_2) species.

Figure 2a shows the calculated lowest-energy profiles for the reactivity of the Fe^{III}(O_2H_2) species in the presence of **S1**, starting from the reactant complex of **RC2**. The lowest energy pathway involves a homolytic O−O bond cleavage, leading to the protonated Cpd II/HO• radical complex, **IC2a**, in which the •OH radical is hydrogen-bonded by the iron-hydroxo moiety. This reaction, which is facilitated by push effects from the thiolate ligand,[4c,5] transpires with a moderate energy barrier of 15.5 kcal/mol. The alternative nucleophilic "assisted" mechanism, whereby the π-component of the double bond of **S1** attacks the ligated HO−OH molecule of **S1** on the distal O_d position, was found to have a much higher barrier of 36.1 kcal/mol (Figure S8). As such, the first step of Fe^{III}(O_2H_2) activation involves **IC2a** formation.

Starting from the **IC2a** (Figure 2a), we considered three competing follow-up reactions. The most favorable pathway in

DOI: 10.1021/jacs.5b02800
J. Am. Chem. Soc. 2015, 137, 7379−7390

the blue curve leads to Cpd I formation, which occurs via the H-abstraction from $Fe^{IV}OH$ by the $^{\bullet}OH$ radical. Cpd I formation is seen to be nearly barrier free. In the alternative follow-up pathways, the coordinated $^{\bullet}OH$ radical either attacks the *meso*-position of the porphyrin (red curve), or the double bond (black curve) in **S1** where it leads to a carbon radical on the C^5 atom of the camphoryl moiety intermediate of **IC2d**, en route to the epoxide product (Figure S10). As can be seen clearly from Figure 2a, *Cpd I formation is clearly favored over the other two pathways, and the reactions of* $Fe^{III}(O_2H_2)$ *will exclusively lead to Cpd I*. Using two other snapshots (Figures S14 and S15), led to the same conclusion as those presented in Figure 2a, namely, that Cpd I formation is much favored over other pathways. We also tested the ZPE corrections for the $Fe^{III}(O_2H_2)$-mediated epoxidation reactions. The ZPE corrections do not change the overall trend and in fact, further reduce the barrier for Cpd I formation (Figure S11). Starting from Cpd I, we further investigated the C═C epoxidation of **S1** by Cpd I based on MD-equilibrated snapshots (Figures S16−S18). In accord with all previous findings,[5] the reaction is stepwise where in the first step Cpd I attacks the C═C bond to form a carbon-based radical intermediate, which undergoes ring closure to the epoxide product. The calculated barrier for the first step is 17.3, 19.1, and 21.6 kcal/mol, depending on the snapshot.

As shown in Figure 2c, H_d of $Fe^{III}(O_2H_2)$ forms a H-bond with the carbonyl oxygen of Gly248 in **RC2**, which is maintained throughout the 20 ns MD simulation (Figure S22). This H-bond is extremely important for the control of the reactivity and regioselectivity of $^{\bullet}OH$ radical. In the QM/MM optimized structure of **IC2a** (Figure 2c), the $^{\bullet}OH$ radical forms a fairly strong H-bond with Gly248 (1.75 Å **IC2a**), *which prevents the rotation of nascent* $H_dO_d^{\bullet}$ *radical*, while the O_p-H_p moiety is in a favorable conformation to form an H-bond with O_d ($Fe^{IV}O_pH_p$---$^{\bullet}O_dH_d$). In this conformation, the $H_dO_d^{\bullet}$ radical is perfectly juxtaposed to abstract a hydrogen atom from $Fe^{IV}O_p-H_p$ to form the Cpd I. Because this juxtaposition is unfavorable for *meso*-site and double bond attack by $H_dO_d^{\bullet}$ radical, these processes entail significant conformational changes and encounter significant barriers.

To gain further insight into the manner whereby the protein controls the $HO^{\bullet}$ radical behavior by a simple H-bonding interaction, we performed a comparative study *in which the above H-bond between* H_d *and Gly248 was artificially severed*. In brief, we run a constrained MD simulation, in which the H_d atom is rotated and pointing down, while the coordinates of the entire $Fe^{III}(O_2H_2)$ and heme units are fixed. This constrained radical **IC3a** and its reactivity patterns are shown in Figure 3, which can be contrasted with **IC2a** in Figure 2. Thus, in the constrained MD-equilibrated structure, the carbonyl oxygen of Gly248 cannot form the H-bond with H_d of the H_2O_2 moiety, but instead Gly248 switches partners and forms an H-bond with the Ala252 (see Figure 3c). In this case, the O−O homolysis results in an upturned $H_dO_d^{\bullet}$ radical, which forms a very strong H-bond with O_p in $Fe^{IV}(H_p)O_p$---$H_dO_d^{\bullet}$ (**IC3a** in Figure 3c). In the **IC3a** conformation, the $H_dO_d^{\bullet}$ radical shows a high reactivity toward addition to the C═C bond (**TS3c**) and porphyrin-ring hydroxylation (**TS3d**), while the formation of Cpd I by abstracting a hydrogen atom from the H_p-O_p bond of $Fe^{IV}O_p-H_p$ (**TS3e**) requires now a much higher barrier compared to the former two pathways (Figure 3a). *It is clear that H-bonding between* H_d *and Gly248 directs* $Fe^{III}(O_2H_2)$ *to form Cpd I in* Figure 2, *while the removal of such H-bonding in* Figure 3 *would have resulted in C═C epoxidation and meso-hydroxylation.*

4.3. Why Does P450cam T252A Perform Efficient Epoxidation of S1? To answer this question we have to consider the full reactivity networks of Cpd 0/**S1** in the mutant enzyme. Figure 4 depicts this network in a triangle that

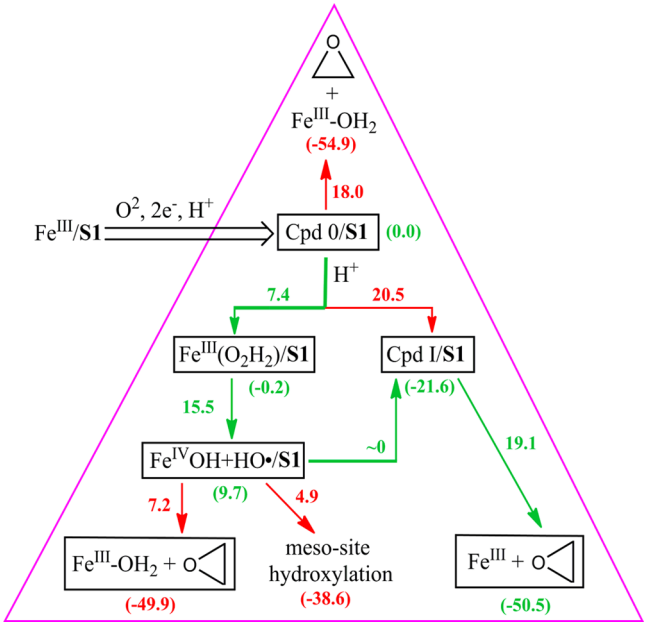

Figure 4. Reaction network of Cpd 0/**S1** in T252A mutant of P450cam. The black arrow penetrating the triangle from the middle left-hand side corresponds to the series of step leading to Cpd 0 (see Scheme 1). The barriers near the respective arrows are in kcal/mol and belong to the rate-determining step in the respective forward transformations, while the energies of species relative to Cpd 0/**S1** (taken as 0.0 kcal/mol) are shown in parentheses. The green pathway is the sole pathway for epoxidation of **S1**, while the red roads are not taken.

corresponds to the evolution of the initially formed Cpd 0/**S1** cluster. Penetrating into the triangle from the left-hand side is the reaction sequence that generates Cpd 0 (see Scheme 1), which is placed in the center of the triangle. Inside the triangle, we have the various processes connecting the species. The green pathway is the least-resistance winning path, while the red pathways are the ones that are "not taken".

Starting with Cpd 0 in the triangle's center, this species can trifurcate to yield an epoxidation product (red) toward the upper corner, or downward to the $Fe^{III}(O_2H_2)$ complex (in green) and/or to Cpd I (in red). It is seen that the lowest barrier, by far, is the one leading to $Fe^{III}(O_2H_2)$, along the green path. The later species forms protonated-Cpd II/$HO^{\bullet}$/**S1** (**IC2a** in Figure 2), which can trifurcate to the *meso*-site hydroxylation (red) product, the epoxide (red) product, or to Cpd I (green). It can be seen that **IC2a** collapses in a virtually barrier free fashion to the Cpd I (green path), while the other two pathways (in red) require sizable barriers. The final oxidant of Cpd I can perform the epoxidation of **S1**.

Thus, our QM/MM calculations reveal a likely exclusive pathway to epoxide formation (in green), in which the $Fe^{III}(O_2H_2)$ species is a requisite intermediate while Cpd I is the sole and final oxidant. Purely based on the reactivity network, we can make two predictions: *(a) if the* $Fe^{III}(O_2H_2)$ *species is not persistent and the* reaction *leads to the release of*

DOI: 10.1021/jacs.5b02800
J. Am. Chem. Soc. 2015, 137, 7379−7390

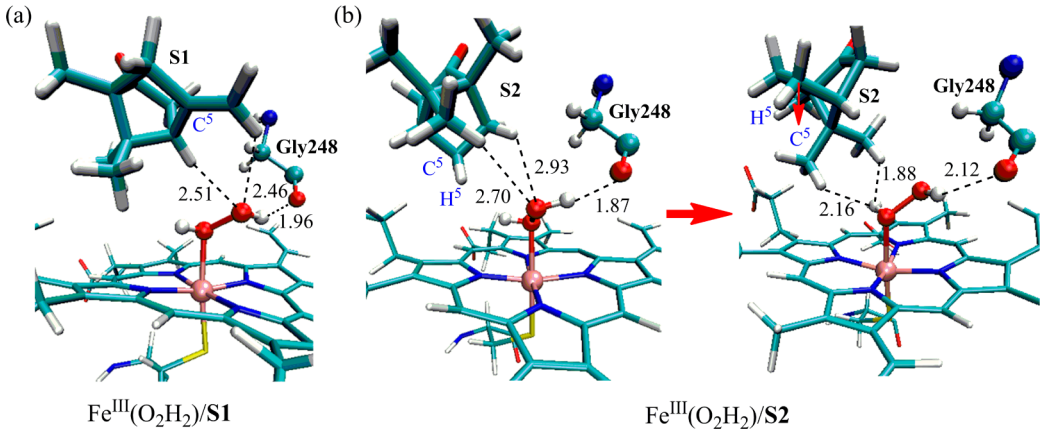

Figure 5. Representative structures of the active site of $Fe^{III}(O_2H_2)$ in the presence of **S1** and **S2** from the MD trajectory: (a) for **S1** and (b) for **S2**, where we show as well the type of configurational change occurring within initial 3 ns of the MD simulations. Key bond lengths are given in angstroms.

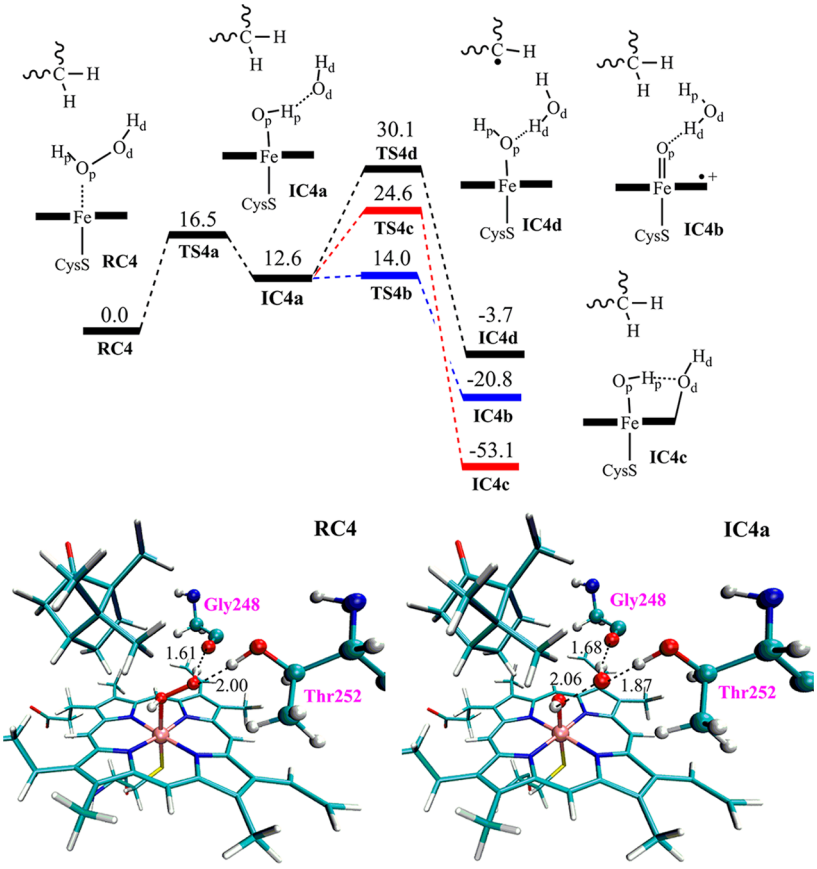

Figure 6. Reactivity of wide-type (WT) P450cam toward **S2** upon H_2O_2 shunting: QM/MM(UB3LYP/B2) relative energies (kcal/mol) for the O–O bond homolysis of $Fe^{III}(O_2H_2)$/**S2** cluster, **RC4**, to yield the **IC4a** intermediate, and its subsequent reactivity patterns. Key intermediates along the reaction energy profile are schematically drawn. The QM/MM optimized structures for **RC4** and **IC4a** are drawn underneath the energy profiles, with key bond lengths in angstroms.

H_2O_2, then there will be no formation of Cpd I and therefore no formation of epoxide product; (2) if the $Fe^{III}(O_2H_2)$ species is sufficiently stable and the reaction *does not lose H_2O_2, then the overall* reaction *will exclusively go through the green pathway to the epoxide product.* Both predictions match the experimental findings that the Cpd 0/**S1** does not release H_2O_2, but leads exclusively to epoxide product in the T252A mutant of P450cam.[9]

4.4. Why Is Camphor (S2) Only Minimally Oxidized in the T252A Mutant of P450cam? As the reaction network in Figure 4 revealed, the only accessible oxidant in the T252A mutant is Cpd I that derives from $Fe^{III}(O_2H_2)$. Therefore, the survival of $Fe^{III}(O_2H_2)$ is key to the overall oxidation reaction. According to our QM/MM calculations, we can already deduce that the poor oxidations of **S2** *should originate in the instability of $Fe^{III}(O_2H_2)$* in the presence of **S2**, such that the conversion of $Fe^{III}(O_2H_2)$ into Cpd I is turned off and **S2** hydroxylation

DOI: 10.1021/jacs.5b02800
J. Am. Chem. Soc. 2015, 137, 7379–7390

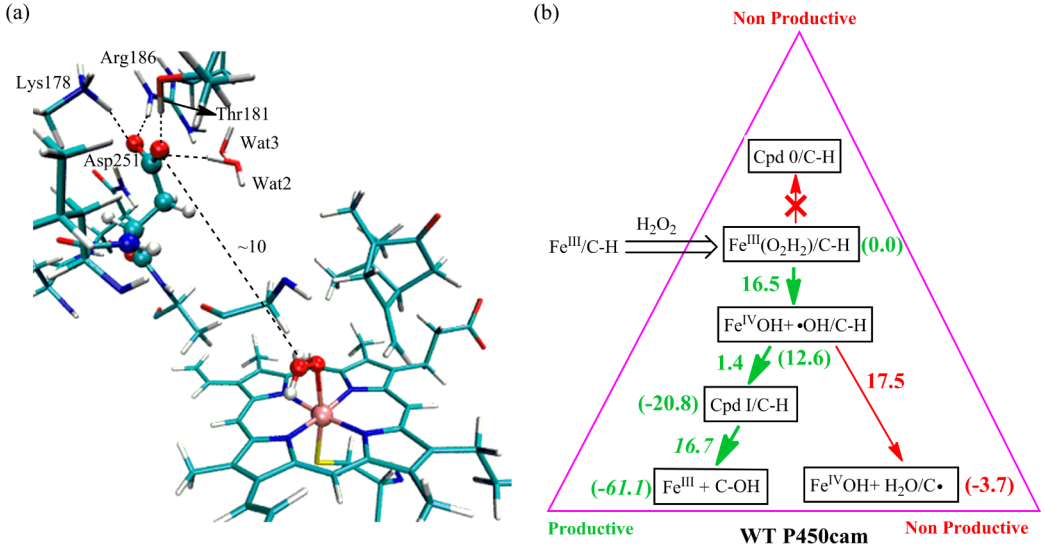

Figure 7. (a) MD equilibrated $Fe^{III}(O_2H_2)$ complex in the WT P450cam. (b) Reaction network for the three oxidants in the hydroxylation of **S2** by H_2O_2 shunting, in the WT P450cam. The barriers near the respective arrows are in kcal/mol and belong to the rate-determining step in the respective forward transformations, while in parentheses we show the energies of the species relative to $Fe^{III}(O_2H_2)$/**S2**. The italicized values for H-abstraction of **S2** are taken from ref 5.

cannot take place. This conclusion deduced from the QM/MM reactivity-network matches the experimental finding that the fate of Cpd 0/**S2** reaction is the loss of H_2O_2.[9]

To ascertain the differences between the $Fe^{III}(O_2H_2)$ intermediates in the presence of **S1** and **S2** in the active site of the mutant enzyme, we investigated the mobility of the two substrates in the presence of the $Fe^{III}(HO_p{-}O_dH)$ intermediate, by means of MD simulations (Figure S22). The representative structures are summarized in Figure 5. Thus, the **S1** substrate forms a relatively stable orientation in the P450cam T252A binding pocket throughout the MD simulations, and is keeping the olefinic moiety, $C^5{=}CH_2$, near and above the H_2O_2 moiety as shown in Figure 5a. Therefore, **S1** barricades the H_2O_2 moiety and prevents its escape from the active site. However, as shown in Figure 5b, the substrate **S2** behaves quite differently. It is seen that **S2** which initially orients its $C^5{-}H$ toward the H_2O_2 moiety, rotates within the initial 3 ns of MD simulations. This mobility of **S2** originates in the greater free space that is created when the bulkier Thr252 is mutated to Ala252. In the upturned structure (Figure 5b, right structure), $C^5{-}H$ is distant from H_2O_2, whereas the bridge methyl groups of **S2** are very close to H_p of H_2O_2. This proximity may sterically destabilize the H_2O_2 or simply prevents its trapping in the enzyme's active site. Thus, unlike **S1**, the **S2** substrate contributes in fact to the instability of $Fe^{III}(O_2H_2)$, and finally to the H_2O_2 release as observed by experiment.[9]

4.5. Why Does the Wild-Type P450cam Enzyme Hydroxylate Camphor (S2) Using H_2O_2 Shunting?

When the WT enzyme is shunted with H_2O_2, the starting point of the oxidation is the $Fe^{III}(O_2H_2)$ complex in the presence of **S2**, which is also the starting point for the T252A mutant. However, in contrast to the T252A mutant enzyme,[8,9,28,59] the WT P450cam was found to be a very efficient H_2O_2-shunt system that produces with **S2** 100% yield of the corresponding hydroxyl camphor product.[28] To understand the difference compared to the T252A mutant, we considered also the structure and reactivity of $Fe^{III}(O_2H_2)$ in the WT P450cam. Figure 6 presents the QM/MM calculated relative energy profile for the reactivity $Fe^{III}(O_2H_2)$ species in the WT P450cam.

Inspection of the $Fe^{III}(O_2H_2)$/**S2** cluster in the WT enzyme, **RC4**, reveals that in addition to the H-bond formed in the T252A mutant between H_d of H_2O_2 and the carbonyl oxygen of Gly248, the WT has an additional H-bond donated by Thr252 to O_d of H_2O_2. This double H-bond in the WT enzyme stabilizes the $Fe^{III}(O_2H_2)$ intermediate compared with the situation in the mutant and helps preventing the escape of H_2O_2, thus potentiating the conversion of this intermediate to Cpd I. The other difference is the substrate mobility in the two enzymes. Thus, as we argued above in T252A, the Ala252 which replaces Thr252 creates more free space in the bonding pocket and allows **S2** to flip upward, and further destabilizes the H_2O_2 ligand by steric repulsion with the bridge methyl groups of **S2** (see Figure 5 above). The result is that the $Fe^{III}(O_2H_2)$ complex in the mutant simply releases H_2O_2. In contrast, the $Fe^{III}(O_2H_2)$ complex of the WT enzyme (**RC4**) is persistent and its **S2** substrate properly juxtapose, so that oxidation can transpire.

As such, O−O bond homolysis leads to **IC4a** (Figure 6) that involves an $H_dO_d^{\bullet}$ radical, which is H-bonded by both Thr252 and Gly248 and oriented in the $H_dO_d^{\bullet}$---$O(H_p)$Fe(IV) manner, precisely as in **IC2a** in Figure 2 in the presence of **S1** (in T252A). Therefore, the radical in **IC4a** is geared toward Cpd I formation in the presence of **S2**. Indeed, as shown in the blue energy profile in Figure 6, the **IC4a** intermediate transforms to Cpd I with a tiny barrier, which is much lower than those for both the $C^5{-}H$ bond hydroxylation and porphyrin ring hydroxylation (black and red curves in Figure 6). Thus, the H_2O_2-shunt of the WT P450cam is remarkably successful due to H-bonding from Gly248 and Thr252, which lends some persistence to the $Fe^{III}(O_2H_2)$ intermediate and steers the $HO^{\bullet}$ radical to form exclusively Cpd I,[28−30] which then hydroxylates **S2**.

To ascertain the identity of oxidant in the shunted WT enzyme, we must further consider also the feasibility of forming Cpd 0/Substrate from $Fe^{III}(O_2H_2)$/Substrate, followed by substrate oxidation by Cpd 0. Inspection of $Fe^{III}(O_2H_2)$/**S2**

DOI: 10.1021/jacs.5b02800
J. Am. Chem. Soc. 2015, 137, 7379−7390

in Figure 7a shows that the carboxylate group of Asp251 is oriented upward due to the salt bridges it maintains with the neighboring residues (Arg 186, Lys 176, etc.[3c,d,5]). Therefore, the Asp251 carboxylate is 10 Å away from the H_2O_2 moiety, and its water channel to this moiety is completely absent. This in turn means that deprotonation of $Fe^{III}(O_2H_2)$ to yield Cpd 0 in the mutant would require significant amount of protein (and water) reorganization, and hence, it would not be facile. Moreover, according to the QM/MM calculations of Altarsha et al.,[27] the deprotonation of $Fe^{III}(O_2H_2)$ in the WT enzyme, requires a barrier of ∼20 kcal/mol,[27] and this is even without consideration of the protein reorganization. Figure 7b shows the reactivity network of $Fe^{III}(O_2H_2)$/**S2** in the WT enzyme. As just argued, the formation of Cpd 0/**S2**(C−H) from $Fe^{III}(O_2H_2)$/**S2**(C−H) is crossed out as being "forbidden". The allowed pathway is the green path, which is nascent from $Fe^{III}(O_2H_2)$/**S2**. As was already shown above, this pathway proceeds via O−O bond homolysis to the $Fe^{IV}OH$---$HO^{\bullet}$ intermediate (**IC4a**), which in turn favors greatly the formation of Cpd I over H-abstraction from **S2** and porphyrin-ring hydroxylation. Cpd I then performs the hydroxylation of **S2**.

4.6. A Revised Catalytic Cycle of P450cam. Based on all these findings, we propose a modified catalytic cycle for P450cam. Starting from Cpd 0, if the second protonation occurs on the distal OH group and a water molecule is liberated, this will directly generate the Cpd I. This process is the well-known coupling process in P450cam catalytic cycle (coupling-I in Scheme 3). However, as we just showed there is

Scheme 3. Updated Catalytic Cycle of P450cam

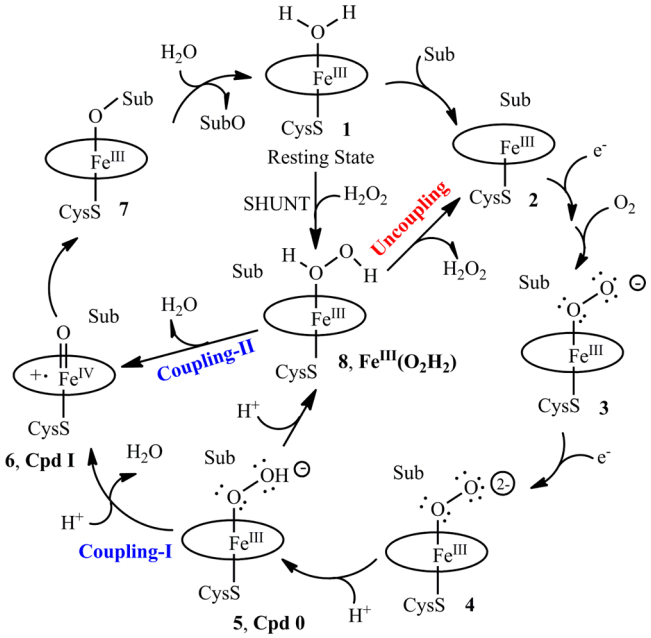

an alterative coupling pathway in P450cam (coupling-II in Scheme 3). Thus, whenever the protonation of the proximal oxygen becomes more favorable over the O−O bond breakage (the rate-determining step in the Cpd 0 → Cpd I transformation), or both processes co-transpire, this will generate the $Fe^{III}(O_2H_2)$ species. $Fe^{III}(O_2H_2)$ will either converts to Cpd I via a O−O homolysis/H-abstraction mechanism or lose H_2O_2 in the uncoupling pathway.

The competition of these two pathways depends on the persistence of $Fe^{III}(O_2H_2)$ intermediate, which is jointly affected by the substrate and the protein. In WT P450cam, H-bonding interactions from Thr252 and Gly248 can sufficiently stabilize $Fe^{III}(O_2H_2)$ intermediate, as we saw in the shunted process (section 4.5), so that $Fe^{III}(O_2H_2)$ can efficiently transform into Cpd I that carries out the oxidation. This behavior in the WT enzyme is not much substrate-dependent. By contrast, in the case of the T252A mutant of P450cam, on the one hand, the replacement of Thr residue by Ala completely removes the H-bond between O_d and Thr252, and on the other, the smaller size of Ala creates more "free space" around the H_2O_2 moiety thereby conferring higher mobility on it as well as on the substrate. In that case, the substrate would play a key role in the stabilization of the $Fe^{III}(O_2H_2)$ intermediate. Thus, as we demonstrated above, the bulkier olefinic moiety of the substrate **S1** tends to barricade the H_2O_2 moiety and prevents its escape from the active site by olefinic moiety, while **S2** (camphor) behaves like a bystander and flips during MD, thus conferring instability (Figure 5) on $Fe^{III}(O_2H_2)$ that consequently loses H_2O_2.

It is believed that the T252A mutant in P450cam turns off the coupling-I process (Cpd 0 → Cpd I). However, this mutation also opens a door to the alternative pathways for Cpd I formation via the $Fe^{III}(O_2H_2)$ intermediate (coupling-II in Scheme 3).

While the details described above concern P450cam, its T252A mutant, and the substrates **S1** and **S2**, nevertheless, the results of this study lead to a general message: *Thus, even when an enzyme and its mutant share the same active species (Cpd I), the final outcome can still be different and will depend on the substrate binding and the H-bond machinery which keeps the oxygen intermediates intact and steers their reactivity, as we found here for $Fe^{III}(O_2H_2)$ in the T252A mutant of P450cam.* This general message may have implications on the intriguing regioselectivity changes observed upon T→A mutations of P450-BM3[10] and P450 Δ2E1.[7] Such changes may still arise from a single oxidant species, Cpd I, which is formed via the coupling-II process in the mutant enzymes, and in the native coupling-I process in the WT enzymes, provided the regiochemical-binding modes for Cpd I/substrate differ in the mutated proteins vs their WT enzymes and are non-interchangeable.[10] It would be worthwhile to address these regioselectivity changes in future QM/MM and MD studies, and generalize our present findings.

5. CONCLUSIONS

This study constitutes a comprehensive QM/MM investigation of the reactions of the potential oxidative pathways in the WT and T252A mutant of P450cam. By generating a full *reactivity network* for the three potential oxidants (Cpd I, Cpd 0, and $Fe^{III}(O_2H_2)$) and all the possible epoxidation pathways, the QM/MM calculations enable us to identify the likely exclusive accessible pathway for the epoxidation of 5-methylenylcamphor (**S1**), in which the $Fe^{III}(O_2H_2)$ species is a requisite intermediate and the Cpd I is the sole and final oxidant. Thus, our QM/MM study reveals the "alternative coupling pathway" in the catalytic cycle of P450cam. In this alternative pathway (coupling-II in Scheme 3), the reaction proceeds via the doublet $Fe^{III}(O_2H_2)$ intermediate, which then generates the ultimate oxidant Cpd I via the O−O homolysis to $Fe^{IV}OH$---$^{\bullet}OH$ followed by H-abstraction and formation of H_2O + Cpd I. The latter then performs substrate oxidations.

DOI: 10.1021/jacs.5b02800
J. Am. Chem. Soc. 2015, 137, 7379−7390

The substrate and protein jointly exert their effects on the stability of $Fe^{III}(O_2H_2)$ intermediate. The substrate may be required to barricade H_2O_2 and confer persistence on $Fe^{III}(O_2H_2)$, as occurred in the T252A mutant of P450cam. The protein on the other hand, can use its hydrogen bonding (H-bonding) machinery to control the reactivity of $Fe^{III}(O_2H_2)$ by forcing the $^{\bullet}OH$ radical to assume a conformation that leads to Cpd I formation, rather than one that leads to the autoxidation of the porphyrin ring, like in Heme Oxygenase. As such, the study not only resolves the longstanding question of the "second oxidant" in P450cam and its mutant, but also reveals that other cases of suspected "second oxidant" activity, may in fact use the new coupling pathway in the catalytic cycle of P450cam enzymes. The present findings have far-reaching implications in the field of P450 enzymes.

■ ASSOCIATED CONTENT

Supporting Information

Optimized geometries, total energies at B2, and Cartesian coordinates of all the structures. The Supporting Information is available free of charge on the ACS Publications website at DOI: 10.1021/jacs.5b02800.

■ AUTHOR INFORMATION

Corresponding Author

*sason@yfaat.ch.huji.ac.il

Notes

The authors declare no competing financial interest.

■ ACKNOWLEDGMENTS

The work is supported by an Israel-Science-Foundation grant (ISF-1183/13) to S.S. This article is dedicated to Prof. Yitzhak Apeloig on occasion of his 70th birthday.

■ REFERENCES

(1) Ortiz de Montellano, P. R. *Cytochrome P450: structure, mechanism, and biochemistry*, 3rd ed.; Kluwer Academic/Plenum Publishers: New York, 2005.
(2) van Eldik, R. *Chem. Rev.* **2005**, *105*, 1917−2722.
(3) (a) Denisov, I. G.; Makris, T. M.; Sligar, S. G.; Schlichting, I. *Chem. Rev.* **2005**, *105*, 2253−2277. (b) Mak, P. J.; Luthra, A.; Sligar, S. G.; Kincaid, J. R. *J. Am. Chem. Soc.* **2014**, *136*, 4825−4828. (c) Vidakovic, M.; Sligar, S. G.; Li, H.; Poulos, T. L. *Biochemistry* **1998**, *37*, 9211−9219. (d) Gerber, N. C.; Sligar, S. G. *J. Biol. Chem.* **1994**, *269*, 4260−4266.
(4) (a) Sono, M.; Roach, M. P.; Coulter, E. D.; Dawson, J. H. *Chem. Rev.* **1996**, *96*, 2841−2887. (b) Groves, J. T. *Nat. Chem.* **2014**, *6*, 89−91. (c) Groves, J. T. *J. Chem. Educ.* **1985**, *62*, 928−931.
(5) Shaik, S.; Cohen, S.; Wang, Y.; Chen, H.; Kumar, D.; Thiel, W. *Chem. Rev.* **2010**, *110*, 949−1017.
(6) Rittle, J.; Green, M. T. *Science* **2010**, *330*, 933−937.
(7) Vaz, A. D. N.; McGinnity, D. F.; Coon, M. J. *Proc. Natl. Acad. Sci. U.S.A.* **1998**, *95*, 3555−3560.
(8) Jin, S.; Makris, T. M.; Bryson, T. A.; Sligar, S. G.; Dawson, J. H. *J. Am. Chem. Soc.* **2003**, *125*, 3406−3407.
(9) Davydov, R.; Perera, R.; Jin, S.; Yang, T. C.; Bryson, T. A.; Sono, M.; Dawson, J. H.; Hoffman, B. M. *J. Am. Chem. Soc.* **2005**, *127*, 1403−1413.
(10) Volz, T. J.; Rock, D. A.; Jones, J. P. *J. Am. Chem. Soc.* **2002**, *124*, 9724−9725.
(11) Cryle, M. J.; De Voss, J. J. *Angew. Chem., Int. Ed.* **2006**, *45*, 8221−8223.
(12) Kerber, W. D.; Ramdhanie, B.; Goldberg, D. P. *Angew. Chem., Int. Ed.* **2007**, *46*, 3718−3721.
(13) Zhou, X. R.; Chen, X.; Jin, Y. Q.; Markó, I. E. *Chem.—Asian J.* **2012**, *7*, 2253−2257.
(14) Coon, M. J.; Vaz, A. D. N.; Mcginnity, D. F.; Peng, H. M. *Drug Metab. Dispos.* **1998**, *26*, 1190−1193.
(15) Nam, W.; Ryu, Y. O.; Song, W. J. *J. Biol. Inorg. Chem.* **2004**, *9*, 654−660.
(16) (a) Chandrasena, R. E. P.; Vatsis, K. P.; Coon, M. J.; Hollenberg, P. F.; Newcomb, M. *J. Am. Chem. Soc.* **2004**, *126*, 115−126. (b) Sheng, X.; Zhang, H. M.; Hollenberg, P. F.; Newcomb, M. *Biochemistry* **2009**, *48*, 1620−1627.
(17) (a) Ogliaro, F.; Visser, S. P.; Cohen; de, S.; Sharma, P. K.; Shaik, S. *J. Am. Chem. Soc.* **2002**, *124*, 2806−2817. (b) Kamachi, T.; Shiota, Y.; Ohta, T.; Yoshizawa, K. *Bull. Chem. Soc. Jpn.* **2003**, *76*, 721−732.
(18) Sharma, P. K.; de Visser, S. P.; Shaik, S. *J. Am. Chem. Soc.* **2003**, *125*, 8698−8699.
(19) Li, C.; Zhang, L.; Zhang, C.; Hirao, H.; Wu, W.; Shaik, S. *Angew. Chem., Int. Ed.* **2007**, *46*, 8168−8170.
(20) Wang, B.; Li, C.; Cho, K. B.; Nam, W.; Shaik, S. *J. Chem. Theory Comput.* **2013**, *9*, 2519−2525.
(21) Park, M. J.; Lee, J.; Suh, Y.; Kim, J.; Nam, W. *J. Am. Chem. Soc.* **2006**, *128*, 2630−2634.
(22) Seo, M. S.; Kamachi, T.; Kouno, T.; Murata, K.; Park, M. J.; Yoshizawa, K.; Nam, W. *Angew. Chem., Int. Ed.* **2007**, *46*, 2291−2294.
(23) Han, A. R.; Jeong, Y. J.; Kang, Y.; Lee, J. Y.; Seo, M. S.; Nam, W. *Chem. Commun.* **2008**, 1076−1078.
(24) Liu, L. V.; Hong, S.; Cho, J.; Nam, W.; Solomon, E. I. *J. Am. Chem. Soc.* **2013**, *135*, 3286−3299.
(25) Kim, Y. M.; Cho, K. B.; Cho, J.; Wang, B.; Li, C.; Shaik, S.; Nam, W. *J. Am. Chem. Soc.* **2013**, *135*, 8838−8841.
(26) Matsui, T.; Unno, M.; Ikeda-Saito, M. *Acc. Chem. Res.* **2010**, *43*, 240−247.
(27) Altarsha, M.; Benighaus, T.; Kumar, D.; Thiel, W. *J. Am. Chem. Soc.* **2009**, *131*, 4755−4763.
(28) Martinis, S. A.; Atkins, W. M.; Stayton, P. S.; Sligar, S. G. *J. Am. Chem. Soc.* **1989**, *111*, 9252−9253.
(29) Joo, H.; Lin, Z.; Arnold, F. H. *Nature* **1999**, *399*, 670−673.
(30) Koo, L. S.; Tschirret-Guth, R. A.; Straub, W. E.; Moenne-Loccoz, P.; Loehr, T. M.; de Montellano, P. R. O. *J. Biol. Chem.* **2000**, *275*, 14112−14123.
(31) The QM/MM was originally conceived in the following: Warshel, A.; Levitt, M. *J. Mol. Biol.* **1976**, *103*, 227−249.
(32) Warshel, A. *Angew. Chem., Int. Ed.* **2014**, *53*, 10020−10031.
(33) Senn, H. M.; Thiel, W. *Angew. Chem., Int. Ed.* **2009**, *48*, 1198−1229.
(34) Lin, H.; Truhlar, D. G. *Theor. Chem. Acc.* **2007**, *117*, 185−199.
(35) Altun, A.; Kumar, D.; Neese, F.; Thiel, W. *J. Phys. Chem. A* **2008**, *112*, 12904−12910.
(36) Bathelt, C. M.; Zurek, J. L.; Mulholland, A. J.; Harvey, J. N. *J. Am. Chem. Soc.* **2005**, *127*, 12900−12908.
(37) Kumar, D.; Thiel, W.; de Visser, S. P. *J. Am. Chem. Soc.* **2011**, *133*, 3869−3882.
(38) Unno, M.; Chen, H.; Kusama, S.; Shaik, S.; Ikeda-Saito, M. *J. Am. Chem. Soc.* **2007**, *129*, 13394−13395.
(39) Schyman, P.; Lai, W. Z.; Chen, H.; Wang, Y.; Shaik, S. *J. Am. Chem. Soc.* **2011**, *133*, 7977−7984.
(40) Sen, K.; Hackett, J. C. *J. Am. Chem. Soc.* **2010**, *132*, 10293−10305.
(41) Wang, B.; Usharani, D.; Li, C.; Shaik, S. *J. Am. Chem. Soc.* **2014**, *136*, 13895−13901.
(42) Wojcik, A.; Broclawik, E.; Siegbahn, P. E. M.; Lundberg, M.; Moran, G.; Borowski, T. *J. Am. Chem. Soc.* **2014**, *136*, 14472−14485.
(43) The substrate affects the P450 cycle in many different ways; e.g.: (a) Sligar, S. G.; Gunsalus, I. C. *Proc. Natl. Acad. Sci. U.S.A.* **1976**, *73*, 1078−1082. (b) Li, H.; Poulos, T. L. *Biochim. Biophys. Acta* **1999**, *1441*, 141−149. (c) Li, H.; Poulos, T. L. *Nat. Struct. Biol.* **1997**, *4*, 140−146.
(44) Schlichting, I.; Berendzen, J.; Chu, K.; Stock, A. M.; Maves, S. A.; Benson, D. E.; Sweet, R. M.; Ringe, D.; Petsko, G. A.; Sligar, S. G. *Science* **2000**, *287*, 1615−1622.

DOI: 10.1021/jacs.5b02800
J. Am. Chem. Soc. 2015, 137, 7379−7390

(45) Olsson, M. H.; Søndergard, C. R.; Rostkowski, M.; Jensen, J. H. *J. Chem. Theory Comput.* **2011**, *7*, 525−537.
(46) Zheng, J.; Altun, A.; Thiel, W. *J. Comput. Chem.* **2007**, *28*, 2147−2158.
(47) Brooks, B. R.; Brooks, C. L., III; MacKerell, A. D., Jr.; Nilsson, L.; Petrella, R. J.; Roux, B.; Won, Y.; Archontis, G.; Bartels, C.; Boresch, S.; Caflisch, A.; Caves, L.; Cui, Q.; Dinner, A. R.; Feig, M.; Fischer, S.; Gao, J.; Hodoscek, M.; Im, W.; Kuczera, K.; Lazaridis, T.; Ma, J.; Ovchinnikov, V.; Paci, E.; Pastor, R. W.; Post, C. B.; Pu, J. Z.; Schaefer, M.; Tidor, B.; Venable, R. M.; Woodcock, H. L.; Wu, X.; Yang, W.; York, D. M.; Karplus, M. *J. Comput. Chem.* **2009**, *30*, 1545−1614.
(48) Vidossich, P.; Fiorin, G.; Alfonso-Prieto, M.; Derat, E.; Shaik, S.; Rovira, C. *J. Phys. Chem. B* **2010**, *114*, 5161−5169.
(49) (a) Sherwood, P.; de Vries, A. H.; Guest, M. F.; Schreckenbach, G.; Catlow, C. R. A.; French, S. A.; Sokol, A. A.; Bromley, S. T.; Thiel, W.; Turner, A. J.; Billeter, S.; Terstegen, F.; Thiel, S.; Kendrick, J.; Rogers, S. C.; Casci, J.; Watson, M.; King, F.; Karlsen, E.; Sjovoll, M.; Fahmi, A.; Schäfer, A.; Lennartz, C. *J. Mol. Struct. (THEOCHEM)* **2003**, *632*, 1−28. (b) Metz, S.; Kästner, J.; Sokol, A.; Keal, T.; Sherwood, P. *WIREs Comput. Mol. Sci.* **2014**, *4*, 101−110.
(50) Ahlrichs, R.; Bär, M.; Häser, M.; Horn, H.; Kölmel, C. *Chem. Phys. Lett.* **1989**, *162*, 165−169.
(51) Smith, W.; Forester, T. R. *J. Mol. Graph.* **1996**, *4*, 136−141.
(52) Bakowies, D.; Thiel, W. *J. Phys. Chem.* **1996**, *100*, 10580−10594.
(53) Becke, A. D. *J. Chem. Phys.* **1993**, *98*, 5648−5652.
(54) Altun, A.; Breidung, J.; Neese, F.; Thiel, W. *J. Chem. Theory Comput.* **2014**, *10*, 3807−3820.
(55) MacKerell, A. D., Jr.; Bashford, D.; Bellott, M.; Dunbrack, R. L., Jr.; Evanseck, J.; Field, M. J.; Fischer, S.; Gao, J.; Guo, H.; Ha, S.; Joseph, D.; Kuchnir, L.; Kuczera, K.; Lau, F. T. K.; Mattos, C.; Michnick, S.; Ngo, T.; Nguyen, D. T.; Prodhom, B.; Reiher, W. E.; III; Roux, B.; Schlenkrich, M.; Smith, J.; Stote, R.; Straub, J.; Watanabe, M.; Wiorkiewicz-Kuczera, J.; Yin, D.; Karplus, M. *J. Phys. Chem. B* **1998**, *102*, 3586−3616.
(56) Billeter, S. R.; Turner, A. J.; Thiel, W. *Phys. Chem. Chem. Phys.* **2000**, *2*, 2177−2186.
(57) (a) Lai, W. Z.; Li, C.; Chen, H.; Shaik, S. *Angew. Chem., Int. Ed.* **2012**, *51*, 5556−5578. (b) Oloo, W. N.; Meier, K. K.; Wang, Y.; Shaik, S.; Münck, E. L., Jr. *Nat. Commun.* **2014**, *5*, 3046.
(58) Danovich, D.; Shaik, S. *J. Am. Chem. Soc.* **1997**, *119*, 1773−1786.
(59) Imai, M.; Shimada, H.; Watanabe, Y.; Matsuhima-Hibiya, Y.; Makino, R.; Koga, H.; Horiuchi, T.; Ishimura, Y. *Proc. Natl. Acad. Sci. U.S.A.* **1989**, *86*, 7823−7827.

DOI: 10.1021/jacs.5b02800
J. Am. Chem. Soc. 2015, 137, 7379−7390